**Supplemental Information**
Neuron, Volume *69*

# RIM Determines $Ca^{2+}$ Channel Density and Vesicle Docking at the Presynaptic Active Zone

Yunyun Han, Pascal S. Kaeser, Thomas C. Südhof, and Ralf Schneggenburger

**Supplemental Data**

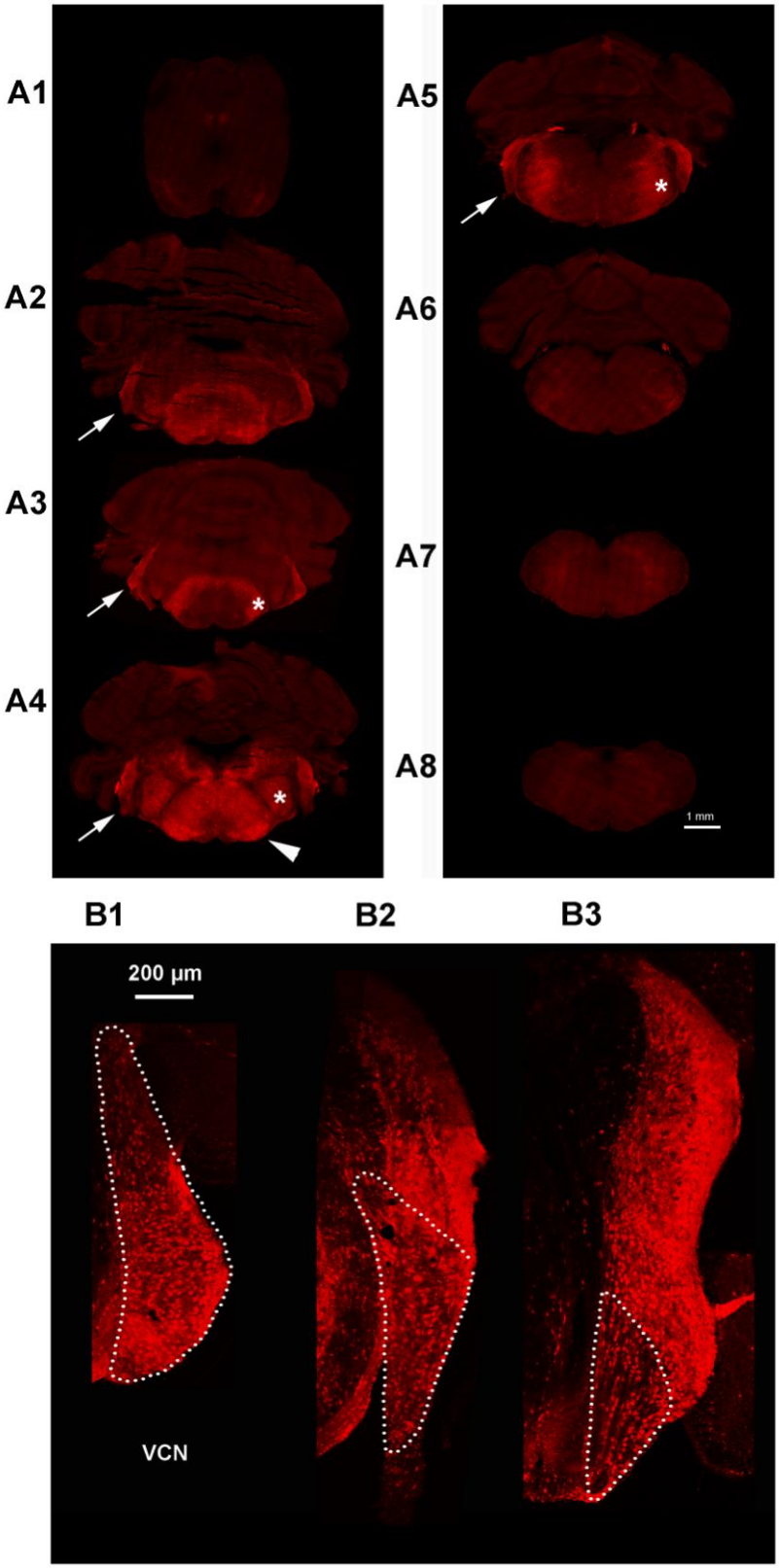


**Figure S1. Cre-activity driven in the brainstem of Krox20+/Cre mice is limited to the lower auditory system and trigeminal nucleus**

This histological analysis examines the spatial distribution of Cre activity in the brainstem of Krox20+/Cre mice (Voiculescu et al., 2000). Krox20+/Cre mice were crossed with tandem-dimer RFP (tdRFP) reporter mice, which express tandem-dimer RFP (tdRFP) following a lox-STOP-lox cassette in the ROSA locus (Luche et al., 2007). In transverse brainstem sections (40 µm) from a P17 offspring of this interbreeding, anti-RFP immunohistochemistry revealed strong Cre activity in the dorsal and ventral parts of the cochlear nucleus (panels A2 - A5; arrow; see also (Farago et al., 2006), in the superior olivary complex including the medial nucleus of the trapezoid body (MNTB) and the lateral superior olive (LSO; A4, arrowhead), and in the trigeminal nuclei (A3, asterisk symbol; see also (Oury et al., 2006). However, Cre activity was absent in the remaining brainstem (Fig. 1A6 - A8), in the cerebellum (A2 - A5), as well as in the midbrain (A1), as expected from the quite selective expression domain of the Krox20 transcription factor in rhombomeres 3 and 5 of the developing brain (Voiculescu et al., 2000).

The panel in (B) shows higher magnification images of the cochlear nuclear complex, proceeding from anterior (B1) towards posterior (B3). Strong expression of tdRFP is observed both in the ventral cochlear nucleus (VCN) where calyx of Held - generating neurons are localized, as well as in the dorsal parts of the cochlear nucleus.

Taken together, the limited expression of Krox20 in neurons that descend from rhombomeres 3 and 5 allowed us to delete floxed alleles quite specifically in the lower auditory brainstem (VCN, MNTB and LSO). The regionally limited Cre expression avoids perinatal lethality that is expected if a more widespread removal occurred, since constitutive RIM1α/RIM2α double KO mice are perinatally lethal (Schoch et al., 2006).

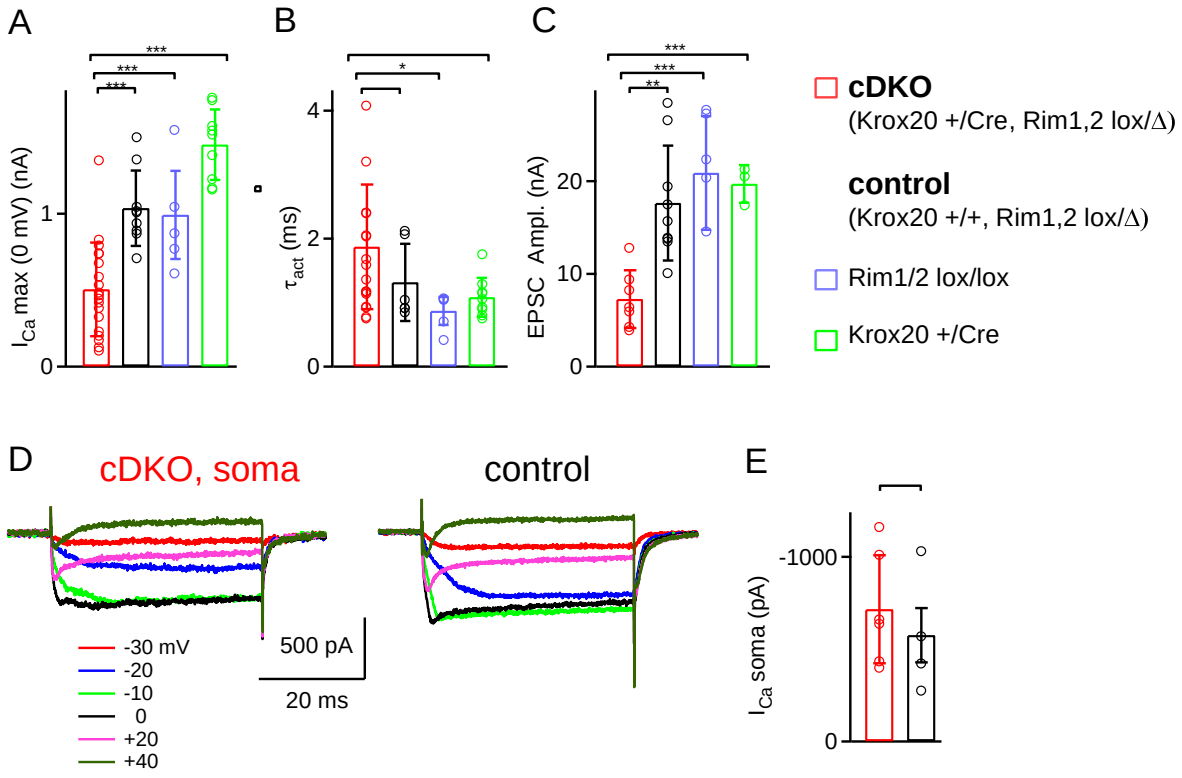


**Figure S2. Comparison of presynaptic $Ca^{2+}$ currents and EPSC amplitudes in RIM1/2 cDKO calyces, and in three types of Cre-positive and Cre-negative control mice, and somatic $Ca^{2+}$ currents**

**A, B, C,** Presynaptic $Ca^{2+}$ currents (A) and the maximal EPSCs following long presynaptic depolarizations (C), were recorded in four genotypes of mice. We compared RIM1/2 cDKO mice (red; all colour codes as in the breeding scheme shown in Supplemental Experimental Procedures), with "control" mice (black symbols; Cre-negative control mice); these two data sets are the same as the ones reported in Fig. 2. In addition, we measured presynaptic $Ca^{2+}$ currents and the maximal EPSC in two additional control mice: First, in homozygous RIM1lox/lox, RIM2lox/lox mice which had never been crossed with Krox20+/Cre mice and which therefore carry both wildtype Krox20 alleles (blue symbols). Second, we measured Krox20+/Cre mice which had never been crossed with the floxed RIM1/2 mice (green symbols).

Comparison of all these four genotypes of mice shows that the presynaptic $Ca^{2+}$ currents (A) and the maximal EPSCs (C) evoked by these $Ca^{2+}$ currents (50 ms depolarizing pulses; these EPSC amplitudes are indicative of the size of the readily-releasable pool) are selectively reduced in RIM1/2 cDKO mice. In constrast, in all control mice, presynaptic $Ca^{2+}$ currents and EPSCs were large, and indistinguishable from each other. Thus, these experiments rule out that expression of Cre-recombinase *per se*, or introducing the floxed RIM1/2 alleles, caused a reduction of the presynaptic $Ca^{2+}$ current (A) or of the readily-releasable pool (C).

In addition, panel B shows an analysis of the activation time-constant of the presynaptic $Ca^{2+}$ channels. In RIM1/2 cDKO calyces (B, red data points and bar), the activation time constant was selectively prolonged ($p < 0.01$), indicating that RIM1/2 might also affect the gating kinetics of presynaptic voltage-gated $Ca^{2+}$ channels.

**D, E.** To test whether RIM1/2 is specifically required for $Ca^{2+}$ channel localization in the nerve terminal as opposed to other neuronal compartments, we measured the voltage-gated $Ca^{2+}$ currents of the soma-dendritic compartment. This was done by recording postsynaptic MNTB cells in which, due to their Cre-activity (see Fig. 1B and Fig. S1), RIM1/2 will be deleted. The postsynaptic $Ca^{2+}$ currents were unchanged (D), with maximal peak amplitudes of 720 ± 290 pA and 570 ± 150 pA in RIM1/2 cDKO neurons and control neurons, respectively ($p = 0.51$; E). This shows that RIM1/2 selectively reduces the $Ca^{2+}$ channel density in the nerve terminal (see Fig. 2).

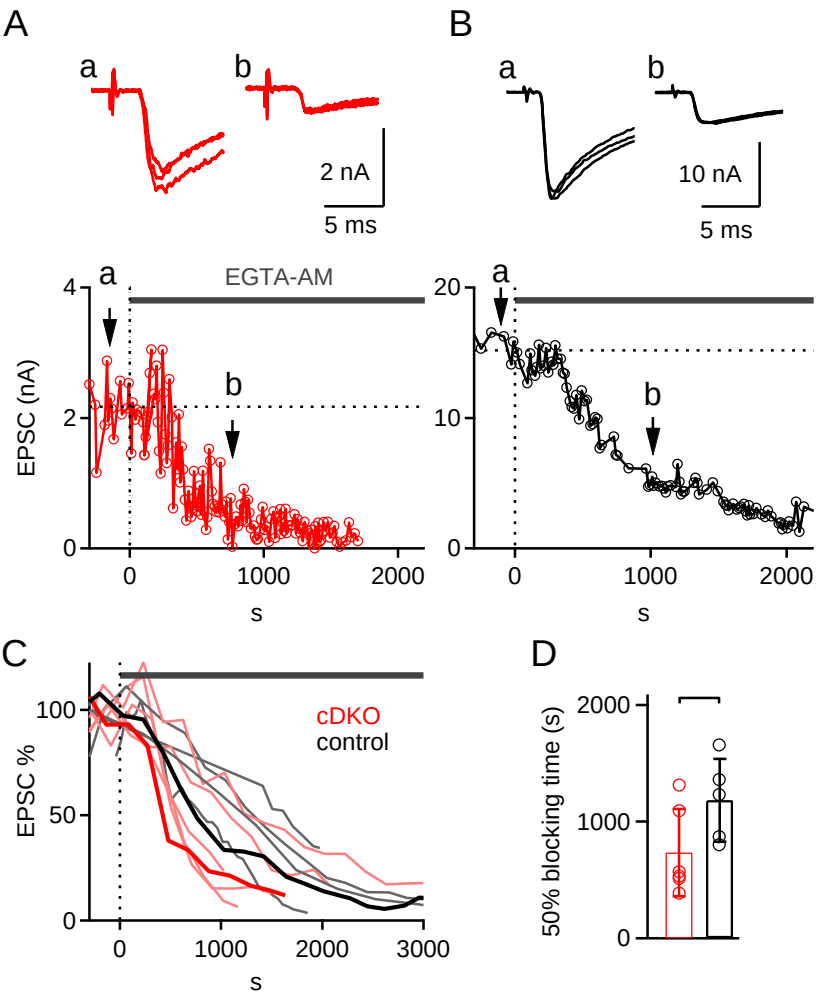


**Figure S3. A trend towards faster block of EPSCs by EGTA-AM in RIM1/2 cDKO synapses**

To test for a reduced spatial coupling between $Ca^{2+}$ channels and readily-releasable vesicles in addition to the experiments shown in Fig. 5, we measured the reduction of transmitter release by the slow $Ca^{2+}$ buffer EGTA-AM. This buffer should lead to the preferential block of release carried by vesicles located further away from $Ca^{2+}$ channels (Borst and Sakmann, 1996; Neher, 1998; Fedchyshyn and Wang, 2005). Therefore, a looser coupling should be detectable by a faster onset of block of EPSCs by EGTA-AM. EPSC were evoked by afferent fiber stimulation at 0.1 Hz, and 200 µM EGTA-AM was added to the bath solution at the indicated times. Panels (A) and (B) show example EPSC traces from a RIM1/2 cDKO calyx of Held synapse (A) and from a control synapse (B). Note the smaller initial EPSC amplitude

in the RIM1/2 cDKO synapse (see also Fig. 1), and the slightly faster development of the block by EGTA-AM. In panel (C), the data from n = 4 recordings for control mice, and n = 5 recordings in RIM1/2 cDKO mice were temporally averaged by binning 200 s intervals, and then plotted normalized to the initial EPSC amplitude before application of EGTA-AM; the traces from the example cells shown in (A, B) are highlighted. Note that in some synapses in RIM1/2 cDKO mice, the block by EGTA-AM developed faster (see leftmost pink traces in C). The time to reach 50% reduction of the EPSC amplitude was interpolated for each recording, and plotted (D). The time to reach 50% block was faster in RIM1/2 cDKO synapses (765 ± 352 s; n = 6) as compared to control synapses (1183 ± 354 s, n = 5); however, this difference was only statistically suggestive (p = 0.073), most likely because of the limited number of recordings. Nevertheless, there was a trend towards a faster block of EPSCs by EGTA-AM, which indicates a looser coupling of readily-releasable vesicle to $Ca^{2+}$ channels, as was also indicated by the experiments in Fig. 5.

**Table S1**

| | docked vesicles adjacent to active zone ("outliers") | | | docked vesicles at active zone | | |
|---|---|---|---|---|---|---|
| | total vesicle number | summed membrane area (µm$^2$) | vesicle density (ves./µm$^2$) | total vesicle number | summed active zone area (µm$^2$) | vesicle density (ves./µm$^2$) |
| RIM1/2 cDKO | 9 | 2.37 | 3.8 | 29 | 1.05 | 27.7 |
| control | 8 | 2.37 | 3.4 | 119 | 1.04 | 114.8 |

This Table summarizes the analysis of docked vesicle found adjacent to the active zone (left columns, "outliers"), and docked vesicles at the active zone, from the data set shown in the ultrastructural analysis of Fig. 6. Note that the summed membrane area adjacent to the active zone (up to 100 nm distance from to the active zone) analyzed in this data set was more than two-fold larger than the summed active zone area. Nevertheless, there were only few "outlier" docked vesicles (9 and 8); therefore, the density of "outlier" vesicles can only be given as average value for the summed adjacent membrane area (3.8, and 3.4 docked vesicles / µm$^2$ for RIM1/2 cDKO and control synapses, respectively). This value is < 5% of the average density of docked vesicles within active zones of wild-type synapses.

**Supplemental Experimental Procedures**

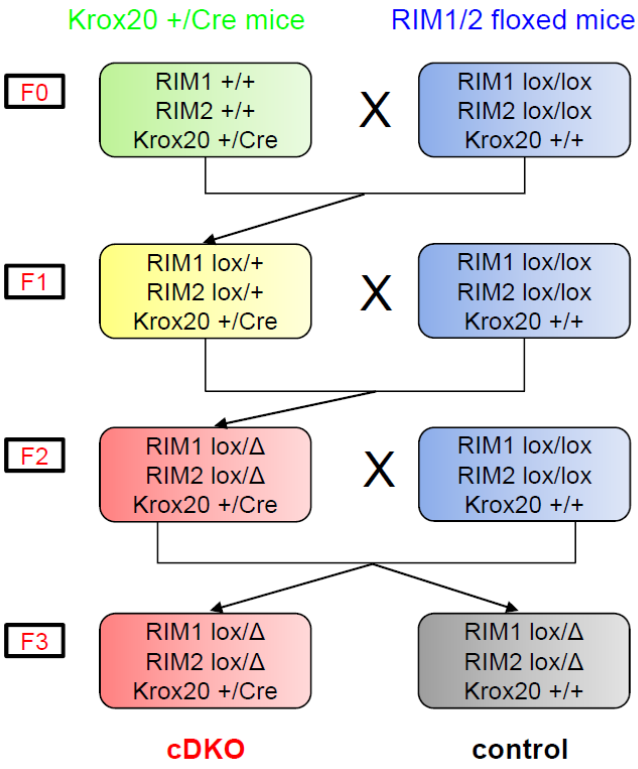


**Breeding scheme for the generation of tissue - specific conditional KO of RIM1 and RIM2**

We crossed heterozygous Krox20+/Cre mice (Voiculescu et al., 2000) with a mouse line that is homozygous for the floxed RIM1 allele (Kaeser et al., 2008), and for the floxed RIM2 allele (Kaeser et al., submitted) ("RIM1/2 floxed mice", indicated by blue boxes). The resulting offspring (F1 generation; yellow) were further crossed against the RIM1/2 floxed mice. Due to germline recombination in the Krox20Cre line (Voiculescu et al., 2000), we obtained RIM1lox/Δ, RIM2lox/Δ mice in the F2 generation. When such mice carry a Cre knock-in allele in the Krox20 locus (red), the second copy of the floxed RIM1/2 alleles is expected to be removed in Cre-expressing cells from ~ E9 onwards, the expression onset of the Krox20Cre transgene (Voiculescu et al., 2000). Therefore, synapses recorded from these mice were called "RIM1/2 cDKO" synapses (for conditional double KO; see red box). Cre-

negative littermate RIM1lox/Δ, RIM2lox/Δ mice were used for control measurements; thus, the "control" mice carried only one functional allele of RIM1 and RIM2. Further control experiments (Fig. S3) showed that these heterozygous control mice had presynaptic $Ca^{2+}$ currents and EPSCs which were indistinguishable from wild-type RIM1/2 mice carrying a Cre allele (see green data points in Fig. S3), and from the RIM1/2 floxed mice (see blue data points in Fig. S3). Thus, removal of one copy of RIM1 and RIM2 did not affect presynaptic function of the RIMs.

**Supplementary Experimental Procedures for electrophysiological methods.**

Pre- and postsynaptic patch-pipettes had resistances of 4 - 7 MΩ and 2 - 4 MΩ, respectively, and series resistance ($R_s$) was compensated by 50% and up to 90%, giving un-compensated $R_s$ values of 5 - 10 MΩ and below 3 MΩ for pre- and postsynaptic recordings, respectively. The remaining $R_s$ error in postsynaptic recordings was corrected with an off-line routine. The liquid junction (LJ) potential between the intra- and extracellular solution was ~ -10 mV; the reported membrane potential values (Fig. 2A, Fig. 2C-H) and holding potential (-70 mV) were not corrected for the LJ potential. Presynaptic $Ca^{2+}$ currents were corrected using a P/5 protocol. The standard pipette (intracellular) solution for pre- and postsynaptic recordings contained (in mM): Cs-gluconate (130), tetra-ethylammonium (TEA) - Cl (20), HEPES (10), Mg-ATP (4 mM), Na-GTP (0.3), $Na_2$-phosphocreatine (5). To this solution, 0.1 mM or 5 mM EGTA were added for pre- and postsynaptic recordings respectively. For presynaptic current-clamp recordings (Fig. 2A), a pipette solution containing 150 mM K-gluconate (instead of Cs-gluconate, and TEA-Cl) was used. The extracellular solution was a standard bicarbonate-buffered Ringer's solution (see Wölfel et al., 2007). To this, 10 µM bicuculline, 2 µM strychnine, 50 µM APV and 100 µM cyclothiazide (CTZ) were added for recording fiber stimulation-evoked EPSCs (Figs 1, 3); 10 mM TEA-Cl, 0.3 mM 4-amino-pyridine, 1.5 µM

tetrodotoxin (TTX), 10 µM NBQX and 50 µM D-APV were added for recording voltage-gated $Ca^{2+}$ currents (Fig. 2C-J), and 10 mM TEA-Cl, 1.5 µM TTX, 50 µM D-APV, 100 µM CTZ and 2 mM γ-DGG were added for paired pre- and postsynaptic recordings and in $Ca^{2+}$ uncaging experiments (Figs 4, 5). All experiments were performed at room temperature (20 - 23 °C).

**Supplementary Experimental Procedures for $Ca^{2+}$ uncaging methods.**

We used single flashes from a DP-10 flash-lamp (Rapp Optoelektronik), coupled into the epi-fluorescence port of the microscope. The presynaptic intracellular solution contained (in mM): 130 Cs-gluconate, 20 TEA-Cl, 20 Hepes, 5 $Na_2$-phosphocreatine, 5 $Na_2$ATP, 0.3 $Na_2$GTP, 0.5 $MgCl_2$, 0.1 fura-2FF (TefLabs, Austin, TX, USA), DM-nitrophen (Calbiochem; 2 mM, with 1.75 mM $CaCl_2$ and 0.5 mM $MgCl_2$ added); pH 7.2, 310 mosmol $l^{-1}$. Calibration of fura-2FF in the presence of 2 mM DM-nitrophen was done as described before (Schneggenburger, 2004).

**Supplementary Experimental Procedures for Immunohistochemistry.**

A P17 mouse resulting from an interbreeding between the Krox20+/Cre mouse line and tdFRP reporter line (Luche et al., 2007) was anesthetized, and then transcardially perfused with 4% PFA. The brain was post-fixed for 12h, and dehydrated in 30% sucrose (PBS) for 48h. Coronal microtome sections (40 µm thickness) were processed free-floating with an anti-RFP antibody (Abcam, Ab62341, 1:500) and an anti-Syt2 antibody (Zebrafish International Resource Center, znp-1, 1:500), and Alexa Fluor 488 goat anti-rabbit, and Alexa Fluor 647 donkey anti-mouse secondary antibodies. Imaging was done under wide-field excitation (Leica DM5500) for overview images (Suppl. Fig. 1A, B) and with a confocal microscope (Leica SP2 invert) for high-resolution (Fig. 1A).

**Supplementary Experimental Procedures for fixation for Electron microscopy.**

A mouse at a time (P11; either control, or RIM1/2 cDKO) was anesthetized and transcardially perfused with PBS followed by 2% paraformaldehyde and 2.5% glutaraldehyde in 0.1 M phosphate buffer (pH 7.4). Transverse brainstem sections were cut with a vibratome (Leica VT1200) at 70 µm thickness, postfixed with 1% osmium tetroxide and 1.5% potassium ferrocyanide in 0.1 M cacodylate buffer, followed by osmium tetroxide in the same buffer and then stained with 1% uranyl acetate. The sections were embedded in Durcupan resin and hardened at 60°C for 48 hours between glass slides. The center region of the MNTB was then cut from the rest of the section, and serially sectioned at 50 nm thickness and collected onto formvar support films on single-slot grids. These were stained with 1.0 % uranyl acetate and lead citrate.

**Supplemental References**

Borst, J. G., and Sakmann, B. (1996). Calcium influx and transmitter release in a fast CNS synapse. Nature *383*, 431-434.

Farago, A. F., Awatramani, R. B., and Dymecki, S. M. (2006). Assembly of the brainstem cochlear nuclear complex is revealed by intersectional and subtractive genetic fate maps. Neuron *50*, 205-218.

Fedchyshyn, M. J., and Wang, L.-Y. (2005). Developmental transformation of the release modality at the calyx of Held synapse. J Neuroscience *25*, 4131-4140.

Kaeser, P. S., Kwon, H. B., Chiu, C. Q., Deng, L., Castillo, P. E., and Südhof, T. C. (2008). RIM1α and RIM1β are synthesized from distinct promoters of the RIM1 gene to mediate differential but overlapping synaptic functions. J Neuroscience *28*, 13435-13447.

Luche, H., Weber, O., Nageswara Rao, T., Blum, C., and Fehling, H. J. (2007). Faithful activation of an extra-bright red fluorescent protein in "knock-in" Cre-reporter mice ideally suited for lineage tracing studies. Eur J Immunol *37*, 43-53.

Neher, E. (1998). Vesicle pools and $Ca^{2+}$ microdomains: New tools for understanding their roles in neurotransmitter release. Neuron *20*, 389-399.

Oury, F., Murakami, Y., Renaud, J. S., Pasqualetti, M., Charnay, P., Ren, S. Y., and Rijli, F. M. (2006). Hoxa2- and rhombomere-dependent development of the mouse facial somatosensory map. Science *313*, 1408-1413.

Schneggenburger, R. (2004). $Ca^{2+}$ uncaging in nerve terminals. In Imaging neurons: a laboratory manual, R. Yuste, F. Lanni, and A. Konnerth, eds. (Cold Spring Harbor, N.Y., Cold Spring Harbor Laboratory Press), pp. 415-419.

Schoch, S., Mittelstaedt, T., Kaeser, P. S., Padgett, D., Feldmann, N., Chevaleyre, V., Castillo, P. E., Hammer, R. E., Han, W., Schmitz, F., *et al.* (2006). Redundant functions of RIM1α and RIM2α in $Ca^{2+}$-triggered neurotransmitter release. EMBO J *25*, 5852-5863.

Voiculescu, O., Charnay, P., and Schneider-Maunoury, S. (2000). Expression pattern of a Krox-20/Cre knock-in allele in the developing hindbrain, bones, and peripheral nervous system. Genesis *26*, 123-126.

Wölfel, M., Lou, X., and Schneggenburger, R. (2007). A mechanism intrinsic to the vesicle fusion machinery determines fast and slow transmitter release at a large CNS synapse. J Neuroscience *27*, 3198-3210.